



Effects of cooling regimes on the microstructural and mechanical properties of the transient liquid phase joints of UNS S32750 super duplex stainless steel/BNi-2/AISI 304 stainless steel

Rouhollah Abdolvand^{1,*} , Masoud Atapour^{1,*}, and Morteza Shamanian¹

¹Department of Materials Engineering, Isfahan University of Technology, 84156-83111 Isfahan, Iran

Received: 7 November 2021

Accepted: 13 January 2022

Published online:
27 January 2022

© The Author(s), under exclusive licence to Springer Science+Business Media, LLC, part of Springer Nature 2022

ABSTRACT

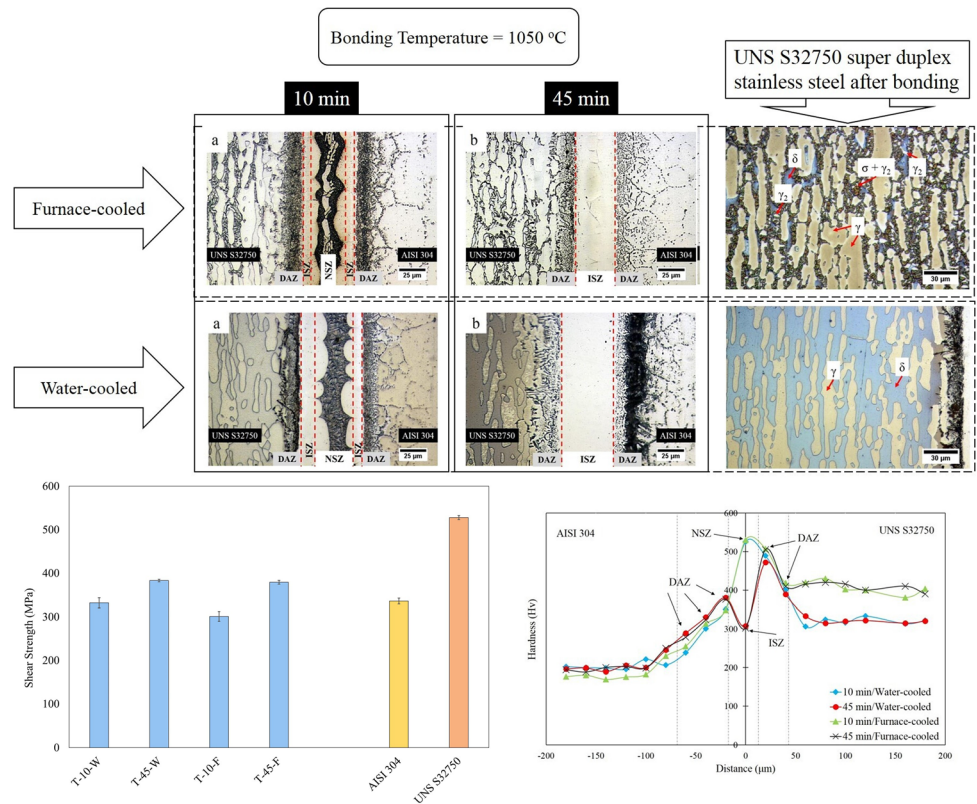
UNS S32750 super duplex stainless steel and AISI 304 stainless steel were transient liquid phase (TLP) bonded using BNi-2 at a bonding temperature of 1050 °C and for two bonding times of 10 and 45 min. After TLP bonding, the samples were subjected to either furnace-cooling or water-cooling regimes. The optical microscope, scanning electron microscope, and energy-dispersive X-ray analysis were employed to investigate the microstructural characteristics of joints, as well as base metals. Moreover, the mechanical properties of the TLP bonds were assessed using microhardness and shear strength examinations. The results showed that the joints fabricated at a bonding time of 10 min exhibited isothermal solidification zone, non-isothermal solidification zone, and diffusion-affected zone, whereas the samples held for 45 min showed a complete isothermal solidification. The only phase in the isothermal solidification zone was γ -Ni solid solution. However, the non-isothermal solidification zone of the water-cooled bond consisted of Ni-rich boride compounds and a γ -Ni solid solution, while Ni-rich and Cr-rich eutectic constituents, as well as Ni₃Si precipitates, existed in the bonding zone of the furnace-cooled sample. Microstructural analysis showed the formation of the σ -sigma phase in the microstructure of the furnace-cooled super duplex stainless steel, which was the primary reason for the increase in the hardness values of the alloy to around 415 Hv. The water-cooled samples, in contrast, did not contain the σ -sigma phase and showed notably lower hardness values (approximately 320 Hv). The non-isothermal solidification zones and diffusion-affected zones of super duplex stainless steels exhibited the highest hardness levels of nearly 525 and 450 Hv, respectively. This work has demonstrated that the joints containing the complete isothermal solidification possessed the highest shear strength, around 380 MPa.

Handling Editor: Naiqin Zhao.

Address correspondence to E-mail: Ruh.Abdolvand@gmail.com; m.atapour@cc.iut.ac.ir

<https://doi.org/10.1007/s10853-022-06928-z>

GRAPHICAL ABSTRACT



Introduction

AISI 304 stainless steel (SS) alloy is one of the most widely used groups of stainless steel alloys [1, 2]. However, despite its versatility and ubiquity, its applications may be limited due to its susceptibility to stress corrosion cracking caused by the alloy's high austenite content [3].

To enhance the resistance of stainless steels to stress corrosion cracking, (super) duplex stainless steel alloys have been developed. These advanced alloys combine the outstanding toughness and strength of austenitic stainless steels with the excellent resistance to stress corrosion cracking of ferritic stainless steels [3]. Better still, due to their lower amount of nickel, their costs tend to be less fluctuating than austenitic stainless steels and nickel-based alloys [4–6]. UNS S32750 super duplex stainless steel

(SDSS) characteristically has a ferrite-to-austenite ratio of 1:1 [7]. This alloy has been rivaling austenitic stainless steels and even nickel-based alloys in many industries, such as the pulp and paper industry [8], where high levels of strength, toughness, and corrosion resistance are required [3, 9].

Dissimilar welding of stainless steel alloys is vital and inevitable not only to lower the final costs of materials and equipment but also to boost the sustainability and adjustability of structures, although it could be challenging. For example, owing to its high alloying elements contents, UNS S32750 SDSS is likely to be difficult to weld via the conventional fusion welding techniques since such processes tend to imbalance the proper ferrite/austenite ratio of the alloy and result in the precipitation of destructive secondary compounds in the weldments [10–12]. However, the formation of secondary precipitates, particularly the σ -phase, deteriorates the properties

of duplex stainless steels and thus must be avoided [13]. Furthermore, chromium carbides are bound to precipitate in the heat-affected zone of austenitic stainless steels if improper fusion welding is used [14].

Transient liquid phase (TLP) bonding has recently been examined by researchers to obtain similar or dissimilar sound joints between various types of stainless steels and other alloys [15–17]. Being a solid-state process, TLP bonding lies between the brazing and diffusion bonding process and offers an ideal combination of features of these two. Compared with the brazed joints, the TLP bonds tend to be noticeably stronger; and unlike diffusion bonding, the TLP process requires a lower amount of pressure and less meticulous surface preparation [18]. Moreover, the TLP bonding process entirely relies on using an interlayer containing certain types of elements (B, Si, and P, for example), which are widely referred to as melting point depressant (MPD) elements. The bonding temperature at which the process is performed must be within a range between the melting point of the interlayer and those of base materials [19]. It is helpful to note that a TLP joint can characteristically be divided into isothermal solidification zone (ISZ), non-isothermal solidification zone (NSZ)—otherwise known as athermal solidification zone (ASZ), and diffusion-affected zone (DAZ).

Several researchers have studied the TLP bonding to create similar or dissimilar bonds between stainless steels and other alloys. Ghaderi et al. [20] TLP bonded Inconel 718 alloy to ultrafine/nanostructured AISI 304L stainless steel at 1050 °C for 5, 15, and 60 min using a BNi-2 interlayer. They observed that eutectic phases in the specimens bonded for 5 and 15 min and concluded that these compounds had adverse effects on the mechanical properties of the joints. Moreover, the isothermal solidification process was fully completed in 1 h. In this condition, the joints were about 1.5 times as strong as the sample held for 5 min. The TLP joints between SAF 2507 SDSS and AISI 420 martensitic stainless steel bonded by BNi-2, at 1050 °C, and for different bonding times up to 60 min, were investigated by Jafari et al. [21]. According to their results, the isothermal solidification process completion was obtained for the samples kept for 60 min at the bonding temperature, and the strength of the joints had a close relationship with the ISZ size. Abdolvand et al. [22] evaluated the properties of TLP joints of UNS S32750 SDSS and AISI 304

stainless steel by means of a BNi-2 amorphous foil at 1050 °C. In this study, diffusion of boron mainly controlled the bonding process. Also, a complete ISZ was obtained at 0.75 h. The impaired mechanical properties of joints bonded for less than this time were linked to the eutectic compounds present within the bonding zones of the joints.

The TLP process offers considerable advantages over the fusion welding methods primarily because base materials are subjected to relatively lower temperatures and thus do not melt during this process [18]. Nonetheless, they are still set to be heat-treated at high temperatures for long periods, to the detriment of their microstructural and mechanical properties, which can be exacerbated if improper heating, cooling, and holding cycles are employed. For instance, slow cooling rates are highly likely to cause the precipitation of detrimental compounds, such as the σ phase, in super duplex stainless steel alloys [23] or abnormal grain growth in austenitic stainless steels [24].

Mosallae et al. [25] used a Ni–P interlayer to yield similar TLP bonds between 2205 duplex stainless steel alloy. The bonding process was carried out at 1150 °C for 60 and 240 min, followed by two subsequent cooling cycles: furnace cooling and water cooling. They reported that the σ phase precipitation happened in the furnace-cooled duplex stainless steel, deteriorating the corrosion properties of the joints. However, a water-cooling cycle helped in preventing this phenomenon. Chiu et al. [11] vacuum brazed 2205 duplex stainless steel in different cooling conditions. According to their findings, the σ phase precipitated in the base metals at cooling rates lower than 0.25 °C/s. They highlighted that the fracture of the slow-cooled brazed bonds occurred at base metals due to the extensive σ phase precipitation in that area. Moreover, the TLP process can trigger grain growth in base metals. Mirzaei et al. [26] used an MBF-20 interlayer to TLP join 304L stainless steel at 1070 °C for 3 to 45 min and noticed that as the bonding time rose, a considerable grain growth occurred in base metals grains, except for the grains of DAZs that were pinned by precipitates.

It appears that the possible effects of the cooling rate on the properties of TLP joints and base materials have been underemphasized in the relevant literature and that a limited number of articles are dedicated to investigating this key factor. Thus, the central focus of the present paper was dedicated to the evaluation

of the impacts of two discrete cooling regimes on the microstructure and mechanical properties of the dissimilar TLP bonds of UNS S32750 super duplex and AISI 304 austenitic stainless steel alloys. As well as that, to propose a suitable bonding cycle for obtaining a sound and sturdy joint with minimal impact on the properties of the base metals, the potential effects of the cooling cycles on the properties of base metals were also studied.

Experimental procedure

In this research, commercial UNS S32750 SDSS and AISI 304 SS sheets (received in hot-rolled and annealed condition) and a BNi-2 foil with a thickness of 50 μm were chosen as the base materials and the interlayer, respectively. The interlayer was selected based on our previous work [22], as well as previous research [18, 27, 28]. The chemical composition of all materials used in this study is summarized in Table 1.

The preparation procedure was as follows: the base alloys were initially cut into samples with dimensions of 40 \times 10 mm, and then their faying surfaces were ground using SiC grinding paper. The cleaning and degreasing processes of the interlayer and base metals were performed within an ultrasonic acetone bath, and then the interlayer was placed and fixed between the parent metals. The bonding process was carried out at a constant temperature of 1050 $^{\circ}\text{C}$ and two bonding times of 10 and 45 min, which were chosen based on our previous study [22], and were selected to study the effect of cooling rate on both NSZ and ISZ.

To assess how different cooling conditions affect the properties of the TLP bonded samples, we selected two different cooling schedules: (1) a slow cooling process within the furnace (with a cooling rate of approximately 0.1 $^{\circ}\text{C s}^{-1}$) and (2) a rapid water-cooling process (with an estimated cooling rate of 200 $^{\circ}\text{C s}^{-1}$). After the bonding process, the preparation of the samples for microstructural investigations

was performed through the conventional metallographic method, and then the cross section of each joint was electro-etched in 10% HNO_3 aqueous solution at 1 V for 10 s. A similar etching condition was used for AISI 304 SS, while UNS S32750 SDSS alloy was electrically etched in a solution containing 40 gr NaOH + 100 gr distilled water, at 5 V, and for 20 s. This solution is recommended for etching duplex stainless steels and for revealing undesirable intermetallic phases, in particular the σ phase, in them [29].

The optical microscope (OM), scanning electron microscope (SEM), and energy-dispersive X-ray spectroscopy (EDS) analysis were used to study the microstructure and estimate the chemical composition of the specimens. The size of DAZs of each sample was measured using the ImageJ software to understand how the size of different zones varies with the bonding temperature and cooling rate, and an average of ten measurements was reported for each zone. The microhardness measurements were taken for each joint with a load of 10 gr applied for 30 s. Additionally, shear strength testing via a fixture, schematically illustrated in Fig. 1, was carried out to evaluate the mechanical performance of the TLP joints and base metals. It should be noted that the samples were coded based on their bonding conditions (Table 2).

Results and discussion

Microstructural evaluation of base metals

The microstructures of AISI 304 SS and UNS S32750 SDSS are shown in Fig. 2. The as-received microstructure of AISI 304 SS consists of the equiaxed grains of austenite with a grain size of $29 \pm 5 \mu\text{m}$. The microstructure of UNS S32750 SDSS contains the δ -ferrite phase (blue phases) and the γ -austenite phase (light brown phases) with a ferrite-to-austenite ratio of 50:50.

Table 1 Chemical composition of the materials and the filler metal

	Chemical composition of the materials (wt%)											
	Fe	Ni	Cr	B	Si	Mo	C	N	Mn	P	S	Cu
UNS S32750	Bal	6.98	26.85	–	1.00	4.76	0.03	0.30	0.56	0.02	0.01	0.97
AISI 304	Bal	8.00	18.50	–	0.75	–	0.07	0.10	2.00	0.04	0.03	–
BNi-2	3.00	Bal	7.00	3.20	4.50	–	0.06	–	–	–	–	–

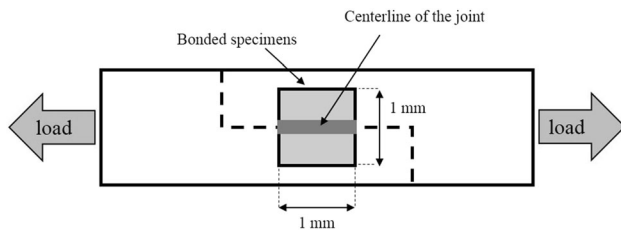


Figure 1 Schematic diagram of the fixture used to measure shear strength.

Effect of cooling cycles on the microstructure of the bonds

Figure 3 displays the microstructures of water-cooled joints. In addition, the optical images of T-10-F and T-45-F samples, as well as the SEM micrograph of T-10-F, are provided in Fig. 4.

The bonding area of T-10-W (Fig. 3a) can microstructurally be divided into three separate parts: isothermally solidified zone (ISZ), non-isothermally solidified zone (NSZ), and diffusion-affected zone (DAZ).

Table 3 compares the EDS results of all regions marked in Figs. 3 and 4. The ISZ of T-10-W is comprised of a single γ -Ni solid solution phase (zone A in Fig. 3). It has been demonstrated that the diffusion of MPD elements governs the formation of ISZ [30]. The formation of ISZ occurred as follows: at 1050 °C, the interactions between the molten interlayer and parent alloys, alongside the MPD elements diffusion, changed the chemical composition of the melt, causing its liquidus temperature to rise. Consequently, the liquid phase started to solidify isothermally. It has been reported that the γ -Ni phase of ISZ forms through heterogeneous nucleation on the base metal surfaces (at a constant temperature) and then grows via an epitaxial growth mechanism [31]. The EDS analysis of ISZ provides evidence that the surfaces of the parent metals dissolved into the interlayer during the bonding process. According to Table 3, higher iron

and chromium contents exist in ISZ when compared to the original amounts of these elements in the interlayer. Moreover, traces of molybdenum, which did not initially exist in the interlayer composition, were detected in the γ -Ni solid solution of ISZ. The formation of diffusion-affected zones (DAZs) also confirms that boron diffused into the base metals. DAZs and their chemical compositions will be discussed later in this paper.

As mentioned, isothermal solidification is a diffusion-controlled process [31]. This means holding time should be sufficient to obtain a complete isothermal solidification. Otherwise, the remaining liquid phase transforms into intermetallic compounds during the cooling stage. The bonding zone of T-10-W consists of NSZ (Fig. 3a) that indicates a 10-min bonding time was insufficient for all the melt to solidify isothermally. The same explanation can be provided for the T-10-F sample whose NSZ was demonstrated in our previous study [22] to be comprised of Ni-rich borides (zone E in Fig. 4) and Cr-rich borides (zone F in Fig. 4). Tiny Ni_3Si precipitates were also detected in the γ -Ni phase of the NSZ (zone G in Fig. 4). Figure 4d displays a magnified image of Ni_3Si precipitates as well.

Nevertheless, it is interesting to note that the microstructure of the NSZ of the water-cooled specimen (T-10-W) and that of the furnace-cooled TLP (T-10-F) bond are markedly different. According to Fig. 3, the NSZ of T-10-W exhibits a cellular structure containing tiny constituents, whereas the NSZ of T-10-F displays the formation of some large and bulky compounds (Fig. 4). Based on the EDS results of the areas shown in Fig. 3, it can be deduced that a γ -Ni solid solution phase (zone B: light dendritic regions) and Ni-rich boride compounds (zone C: dark, blocky, and dendritic regions) exist in the NSZ of T-10-W. Once the rapid water-cooling cycle started, the γ -Ni nuclei formed and then grew on the melt/ISZ interface. However, the growth of these nuclei was hindered due to the high cooling rate in water, which explains why the γ -Ni solid solution particles in the NSZ of the T-10-W sample are smaller in size when compared to their furnace-cooled counterparts. It should be noted that while EDS analysis fails to detect boron in the phases formed in NSZ, it can be used to confirm the formation of boride compounds in this region. The following explains the rationale behind this assumption: the Ni–B phase diagram indicates that boron has almost no solubility

Table 2 Bonding conditions and codes of joints

Sample	Temperature (°C)	Time (min)	Cooling environment
T-10-W	1050	10	Water
T-45-W	1050	45	Water
T-10-F	1050	10	Furnace
T-45-F	1050	45	Furnace

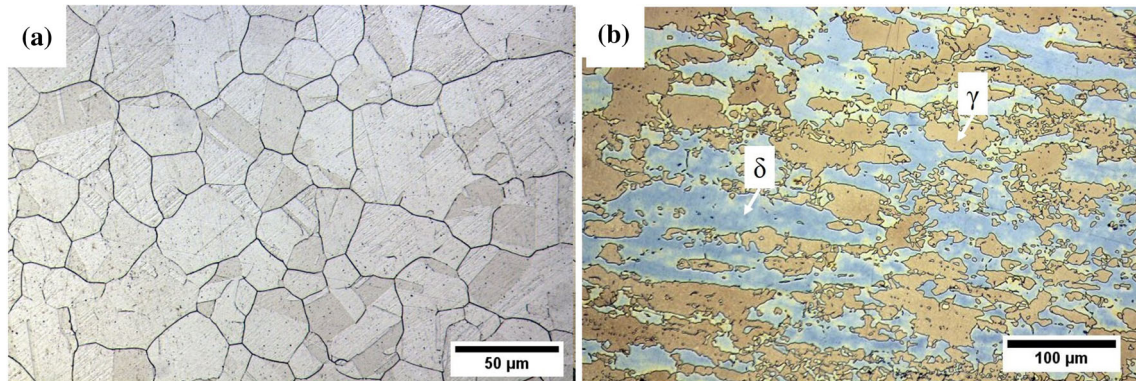


Figure 2 Optical micrographs of **a** AISI 304 stainless steel and **b** UNS S32750 super duplex stainless steel. The γ and δ denote austenite and ferrite phases, respectively.

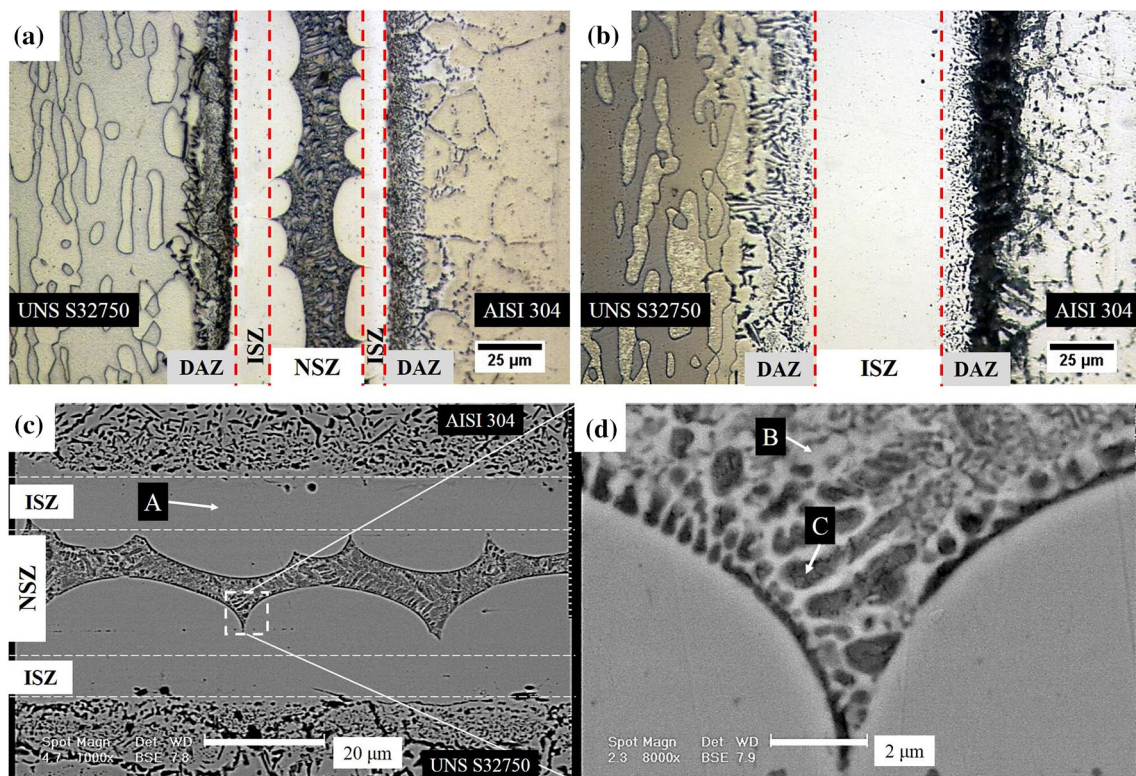


Figure 3 **a, b** Microstructures of the T-10-W and T-45-W, respectively; **c, d** SEM images of the bonding zone of T-10-W.

in nickel [32], meaning that during the growth of the γ -Ni phase in the NSZ, the rejection of boron into the liquid phase occurred and increased the boron content of the remaining melt. Accordingly, the remaining molten phase solidified, and the micron-sized Ni-rich borides and γ -nickel solid solution formed. Furthermore, the insignificant amount of silicon in the NSZ compounds of T-10-W (approximately 1.5 wt%) is insufficient for silicide phases to precipitate, which indicates that only boride phases could form within

the NSZ of T-10-W and that there was no possibility for the formation of silicide compounds. Moreover, it was concluded that silicon has dissolved in the γ -nickel solid solution (and not boride compounds) since it has no solubility in borides either [33].

Unlike the NSZ of the furnace-cooled sample (T-10-F), no Cr-rich boride was detected in the NSZ of the water-cooled bond (T-10-W). The absence of Cr-rich borides in the water-cooled bond was attributed to the rapid solidification process used for this

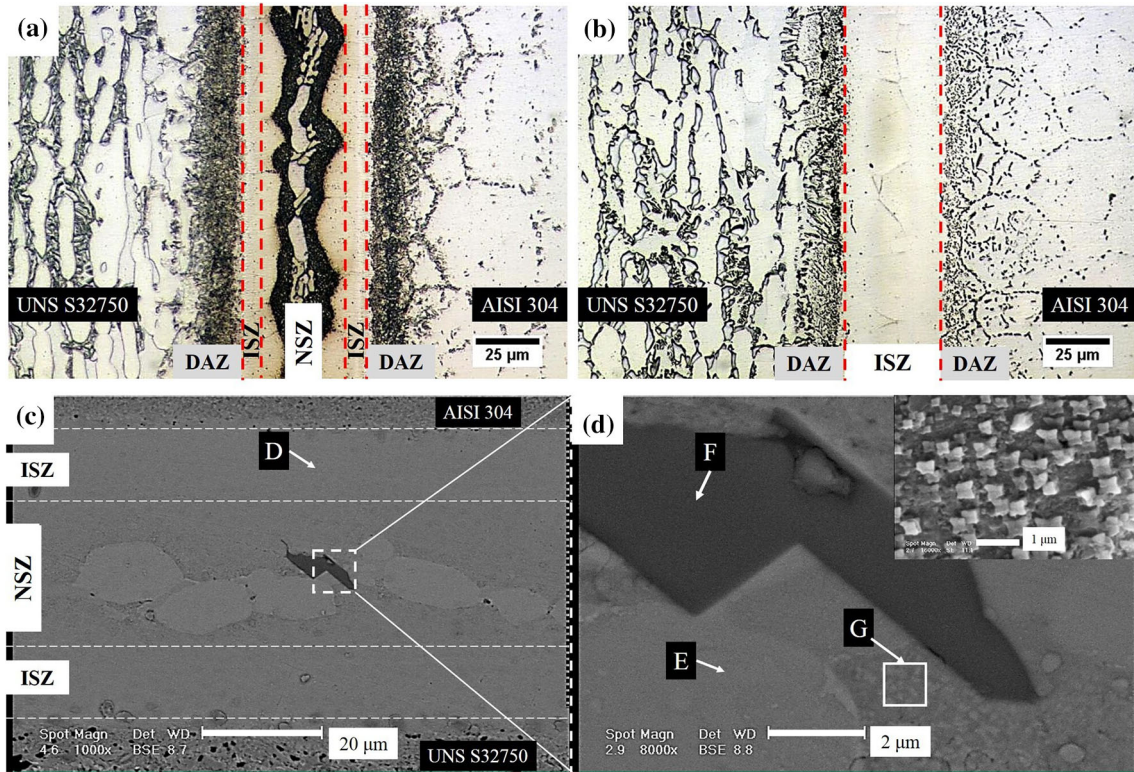


Figure 4 a, b Optical micrographs of the T-10-F and T-45-F, respectively. c, d SEM images of the bonding zone of T-10-F. A magnified SEM image of the area G is presented in the top-right corner of (d).

Table 3 Chemical composition of various areas marked in Figs. 3 and 4

Zone	Element (wt%)					Proposed phases	
	Ni	Cr	Si	Fe	Mo		
Water-cooled	A	70.6	8.73	2.52	14.04	4.11	γ -Ni solid solution (in ISZ)
	B	68.21	10.85	6.21	12.73	2	γ -Ni solid solution (in NSZ)
	C	84.56	6.35	1.49	6.1	1.5	Ni-rich boride
Furnace-cooled	D	74.14	10.05	8.37	3.33	4.11	γ -Ni solid solution (in ISZ)
	E	86.69	5.59	2.21	5.51	–	Ni-rich boride compounds
	F	11.00	75.33	1.73	4.03	7.91	Cr-rich boride compounds
	G	78.59	5.31	3.75	8.87	3.48	Ni_3Si precipitate

specimen. It has been well documented that the formation of Cr-rich boride compounds occurs as the result of the growth of Ni-rich borides and the subsequent rejection of chromium into the remaining melt [22, 27, 30]. By comparing the size of the Ni-rich borides in the NSZ of T-10-W and T-10-F TLP bonds, it is then inferred that the rapid solidification associated with the water-cooling regime impeded the growth of the Ni-rich borides, as well as the rejection of chromium. Therefore, it is reasonable to conclude that the Cr-rich borides did not form in the NSZ of the T-10-W joint.

Another important difference between the NSZs of T-10-W and T-10-F (Figs. 3d, 4d, respectively) is the absence of Ni_3Si precipitates in the former. It has been reported that during the slow cooling process, such as furnace cooling, Ni_3Si deposition occurs in the γ -Ni matrix through a solid-state phase transformation due to the difference between the solubility of silicon in nickel at high bonding temperature (around 8 wt% at 1050 °C) and room temperature (approximately 4 wt%) [32]. The microstructural analysis of the T-10-W sample confirms that the Ni_3Si was absent in the water-cooled bond. Furthermore, the EDS

results of zone B in Fig. 3 suggest that the silicon content of the γ -Ni phase of the NSZ of T-10-W (6.21 wt%) is comparatively higher than the room temperature solubility of silicon in nickel (4 wt%). Considering no Ni_3Si precipitated in this region, it can be readily concluded that the γ -Ni solid solution phase in the NSZ of T-10-W is supersaturated.

The primary objective of performing the TLP bonding process is to reach a eutectic-free joint. In this work, the isothermal solidification completion was attained at a holding time of 45 min. The microstructures of fully isothermally solidified bonds in T-45-W and T-45-F samples are presented in Figs. 3b and 4b, respectively. The ISZs of both joints have a similar microstructure and chemical composition. This similarity is linked to the nature of the isothermal solidification phenomenon itself, meaning that it is not affected by changing the cooling rate at all. The γ -Ni solid phase is the only phase found in the ISZs of both bonds (Table 3).

Moreover, the completion of isothermal solidification is accompanied by the precipitation of some micro-constituents in the areas adjacent to the inter-layer/base material interface [17]. These regions are named diffusion-affected zone (DAZ) and can impair the mechanical properties of TLP bonds due to containing detrimental, brittle, and hard precipitations [34, 35].

As it was mentioned, the DAZs in TLP bonds are believed to be the direct result of the diffusion of MPD elements (boron and silicon in this study) into parent materials at a constant bonding temperature. This is confirmed since the intermetallic constituents are also present in the DAZs of the water-cooled samples (T-10-W and T-45-W). In a previous study, we have already demonstrated that in the furnace-cooled samples, Cr–Fe-rich borides and carb-borides formed in the DAZ of AISI 304 SS, whereas the DAZ of UNS S32750 SDSS consisted of borides of various elements (Ni, Fe, Cr, and Mo) and boron nitride [22].

Figure 5 displays the FE-SEM microstructures of the DAZ of the T-45-W sample, and Table 4 summarizes the EDS results of the regions marked in Fig. 5. High chromium and iron contents in zone H and high amounts of chromium, iron, and nickel in zone I suggest that Cr–Fe-rich borides and Cr–Fe–Ni-rich borides formed in these regions, respectively. Further, the considerable amounts of chromium and molybdenum in zone J confirm the presence of Cr–Mo-rich boride compounds.

The high proportion of boron, nitrogen, chromium, and iron in zone K indicates that there are Cr–Fe-rich borides and boron nitrides in this zone. It should be noted that UNS S32750 SDSS contains nitrogen, which is a strong boride-forming element [28]. Therefore, the formation of boron nitride in the DAZ of SDSS can be explained based on this thermodynamic fact that boron nitride has lower Gibbs free energy than other carbides and nitrides [28]. However, the formation of nitride compounds is highly likely to be limited due to the low amount of nitrogen of UNS S32750 SDSS.

As shown in Fig. 5b, the DAZ of AISI 304 SS of the T-45-W sample consists of different types of compounds with blocky and needle-like morphologies. As per the EDS analysis in Table 4, Cr–Fe-rich borides and Cr–Fe-rich carbo-borides formed in the DAZ of AISI 304 SS. A relatively high carbon content in AISI 304 SS (0.07 wt%), as well as the diffusion of boron into AISI 304 SS, promoted the formation of carbo-boride compounds in the AISI 304 SS side. It needs to be considered that when boron diffuses into the AISI 304 SS base metal, the solubility of carbon in the alloy will drop, which can result in the formation of the carbo- or carbo-boride compounds [36].

The bar chart in Fig. 6 compares the average size of the DAZs of all bonded samples. In both water-cooled and furnace-cooled joints, the size of DAZ of AISI 304 is markedly larger than that observed for the UNS S32750 SDSS. This disparity is because boron diffuses at a higher rate in AISI 304 SS than it does in UNS S32750 SDSS [22]. Moreover, the width of DAZ is inextricably linked to the length of the bonding time since longer holding times allow higher amounts of boron to travel in the farther areas within the base metals. This, in effect, results in the formation of more boride-based compounds in wider areas of the base metals, hence the larger DAZs. According to Fig. 6, the difference between the sizes of the DAZs of SDSS in all joints is negligible, even though the DAZs of the AISI 304 SS of the furnace-cooled joints are wider. This difference is attributed to the slow cooling rate of the furnace-cooling regime. As explained, at the holding temperature, isothermal solidification and diffusion of alloying elements in the parent alloys simultaneously began and then proceeded. However, while the former ceased once the cooling process started, the latter uninterruptedly continued in the furnace-cooling sample; as a result,

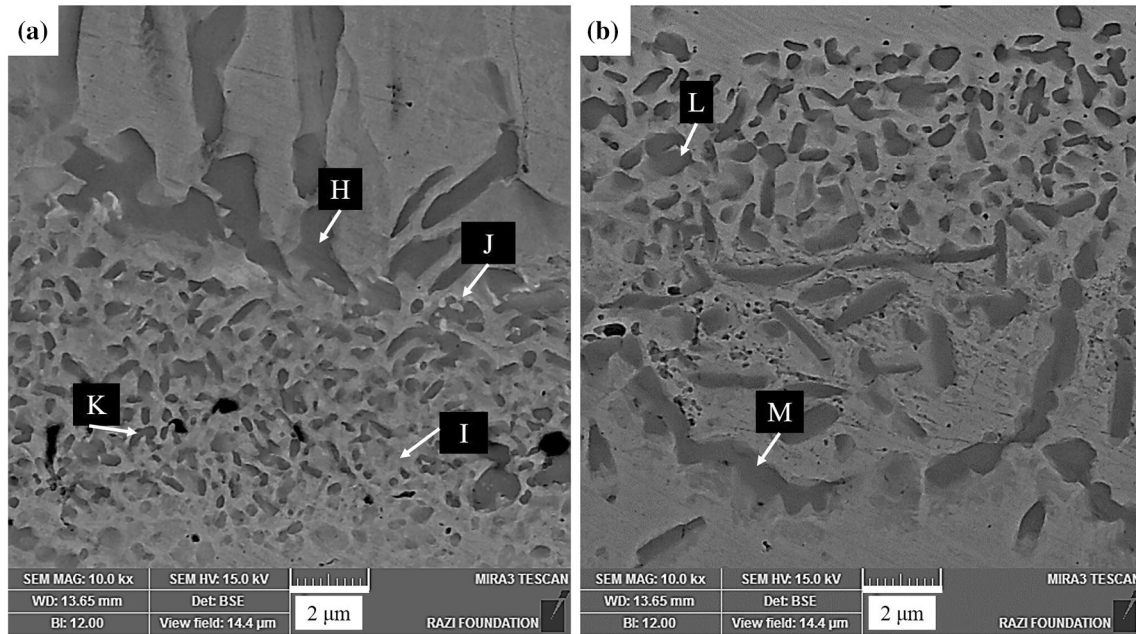


Figure 5 FE-SEM microstructures of **a** diffusion-affected zone of UNS S32750 super duplex stainless steel and **b** diffusion-affected zone of AISI 304 stainless steel of the T-45-W joint.

Table 4 Chemical composition of the regions marked in Fig. 5

Zone	Element (wt%)								Proposed phases
	B	Ni	Cr	Si	Fe	Mo	C	N	
H	21.26	17.15	28.46	0.24	27.24	2.19	–	3.46	Cr-Fe-rich borides
I	16.96	25.02	25.26	0.42	26.34	1.4	–	4.6	Fe-Cr-Ni-rich borides
J	40.89	4.54	25.64	0.98	8.39	19.56	–	–	Cr-Mo-rich borides
K	19.06	7.05	28.15	0.2	27.24	1.9	–	16.4	Cr-Fe-rich borides and boron nitride
L	25.47	12.84	25.43	0.31	15.33	0.88	19.74	–	Cr-Fe-rich borides/carbo-borides
M	22.59	1.37	28.96	0.15	20.41	–	26.52	–	Cr-Fe-rich borides/carbo-borides

more participates, i.e., a wider DAZ, formed in the base metals.

Effect of cooling conditions on the base materials

One of the main problems of the TLP process is that the base metals can be negatively affected during the heating or cooling cycles. Therefore, after the TLP process, the microstructures of the base metals were investigated. Figure 7a, b shows the microstructure of UNS S32750 SDSS of the TLP samples cooled in the furnace. As can be seen, the slow furnace-cooling treatment (cooling rate: approximately 0.1 °C s⁻¹) has disturbed the austenite-ferrite balance and has

pronouncedly changed the microstructure of UNS S32750 SDSS, in which only the δ–delta ferrite and γ–gamma austenite phases existed initially (Fig. 2b). The δ–delta ferrite and γ–gamma austenite phases (light blue and light brown regions, respectively) can be seen in the microstructure of duplex super stainless steel of all TLP joints (Fig. 7). However, it seems that a markedly lower proportion of ferrite exists in the furnace-cooled SDSS base metals when compared to their water-cooled counterparts, while a new dark brown/tan phase can be observed in the SDSS of the T-45-F TLP joint (Fig. 7a, b). The volume fraction of ferrite in the furnace-cooled SDSS is approximately 8%, notably lower than the alloy’s original ferrite content (50%). This indicates that secondary

Figure 6 Width of diffusion-affected zones (DAZ) of different TLP joints. W and F denote water-cooled and furnace-cooled regimes, respectively.

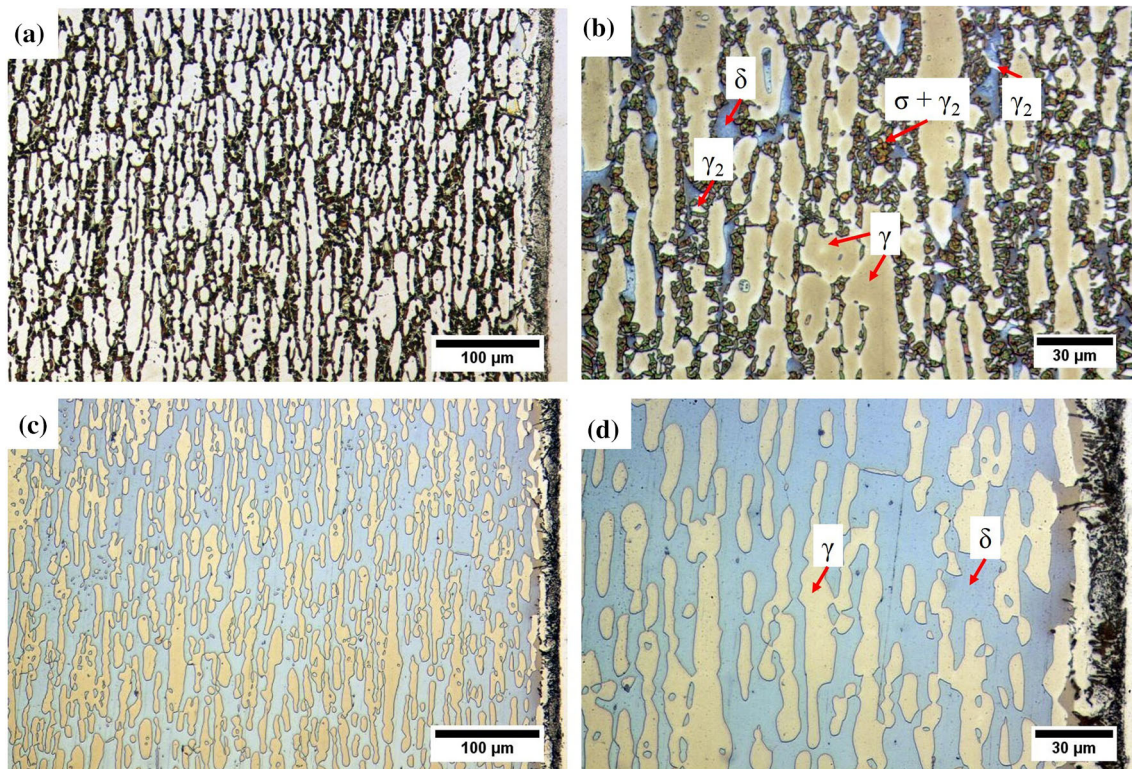
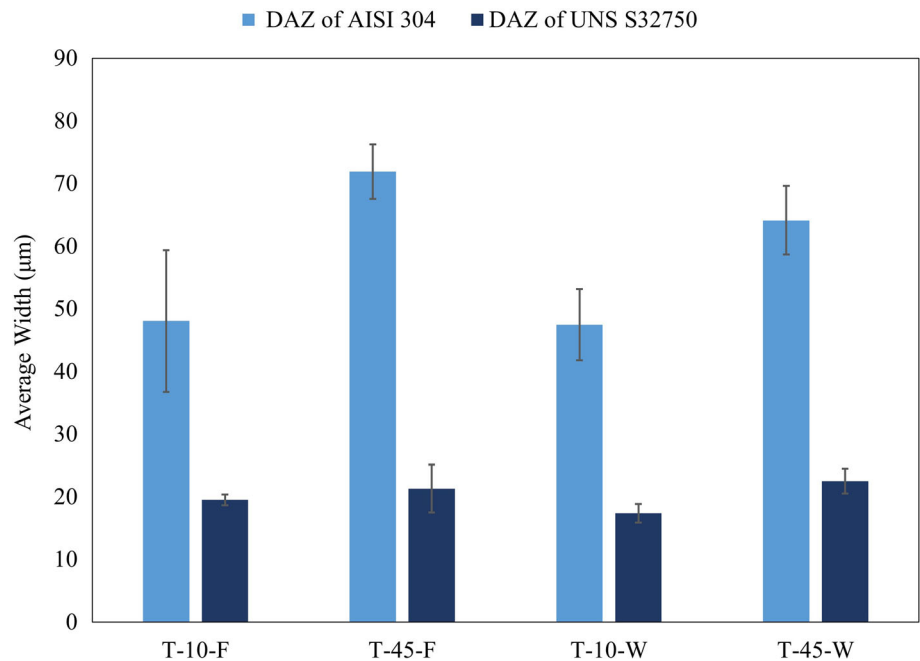


Figure 7 Microstructures of **a, b** furnace-cooled and **c, d** water-cooled UNS S32750 super duplex stainless steel. The γ , δ , σ , and γ_2 symbols denote the austenite, ferrite, sigma, and secondary austenite phases, respectively.

intermetallic phases, such as the σ -phase and χ phase, have precipitated within the furnace-cooled alloys [7, 23].

Figure 8 illustrates the equilibrium phase fraction for UNS S32750 SDSS as a function of temperature [37] and the calculated continuous-cooling-transformation (CCT) diagram of this alloy [13]. At a holding

temperature of 1050 °C, the δ phase fraction should be approximately 40% (Fig. 8a), which is near to the initial ferrite content of the alloy. However, at the temperature range below the bonding temperature (< 1000 °C), the phase balance will be disturbed, and the secondary phases will precipitate in the δ -ferrite phase. Among these phases, the σ phase is the most notorious due to its highly deleterious effects on the corrosion resistance and mechanical properties of super duplex stainless steel alloys [13]. It has been reported that this phase precipitates along the δ/γ interphase boundaries and through the $\delta \rightarrow \sigma + \gamma$ eutectoid phase transformation [38]. Furthermore, its formation is likely to trigger the precipitation of the secondary austenite phase (γ_2) as it causes the depletion of the δ -ferrite phase from the ferrite stabilizer elements (such as chromium and molybdenum). This eventually destabilizes the ferrite phase and facilitates the ferrite transformation into the γ_2 phase. The γ_2 too is prone to corrosion due to its inadequate chromium and molybdenum contents [39].

- The CCT diagram (Fig. 8b) suggests that the critical cooling rate for the formation of 1% σ phase in UNS S32750 SDSS is approximately $0.4 \text{ }^\circ\text{C s}^{-1}$, meaning the σ phase (as the most stable secondary phase in the temperature range of 650–950 °C (Fig. 8a) [13]) was bound to form in the furnace-cooled SDSS. The SEM microstructure of the furnace-cooled SDSS is given in Fig. 9, and the EDS results of the identified phases are listed in Table 4. While the Ni-rich austenite phase appears slightly lighter than the δ -ferrite phase

[(Cr, Mo)-rich phase], the σ phase [(Cr, Mo)-rich phase] is strikingly lighter than both ferrite and austenite phases. As it has been previously reported in the literature, two different morphologies of the σ phase can be identified in Fig. 9: the blocky σ phase, which precipitates at the δ/γ phases interfaces, and the skeleton-like σ phase, which forms within the δ -ferrite grains [39]. As shown in Fig. 9, the γ_2 islands, which look darker than other phases, can also be observed in the adjacent areas of the skeleton-like σ phase. This observation confirms that the aforementioned eutectoid phase transformation occurred during the furnace cooling (Table 5).

In contrast, the SDSS of the water-cooled joint (T-45-W) contained $41 \pm 5\%$ δ -ferrite phase without apparent secondary phase precipitation. Such a ferrite content in UNS S32750 SDSS is sufficient and desirable to reach excellent mechanical performance and corrosion resistance [7].

Figure 10 shows the optical microstructures of AISI 304 SS of the T-45-F and T-45-W TLP bonded specimens. Grain growth is the most important issue that has occurred in the AISI 304 SS side. The average grain sizes of the furnace-cooled and water-cooled AISI 304 SS alloys are 42 ± 4 and $35 \pm 3 \text{ }\mu\text{m}$, respectively. Due to its more prolonged exposure to high temperatures, the furnace-cooled sample has a greater grain size than the water-cooled one. Also, some indications of abnormal grain growth, such as the convex grain boundaries and markedly large grains ($> 60 \text{ }\mu\text{m}$) [24], can be observed in the

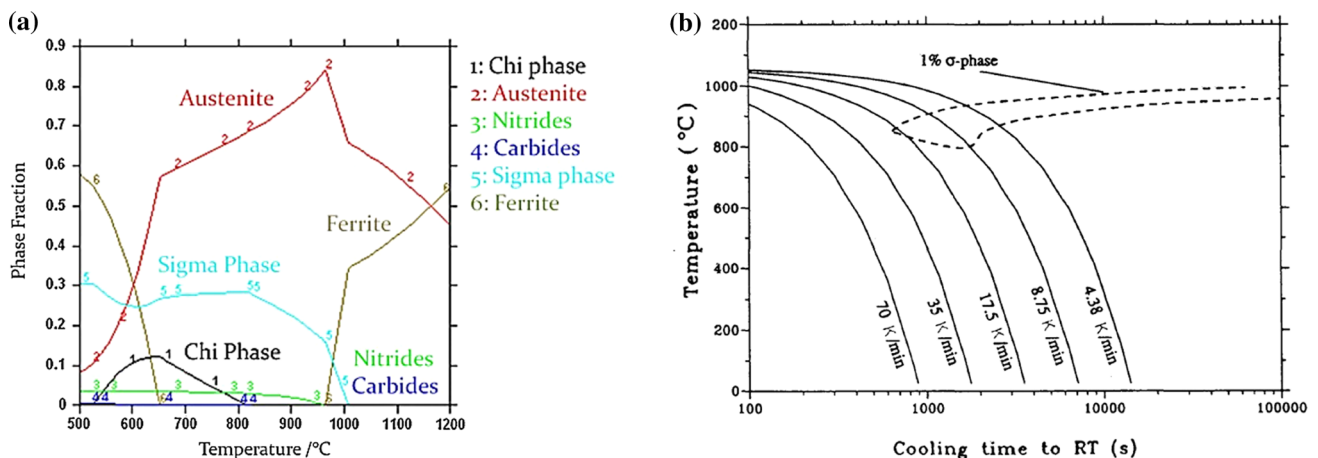


Figure 8 a Thermodynamic calculation of equilibrium phase fraction for UNS S32750 super duplex stainless steel versus temperature [37], and b the continuous-cooling-transformation (CCT) diagram of the alloy [13].

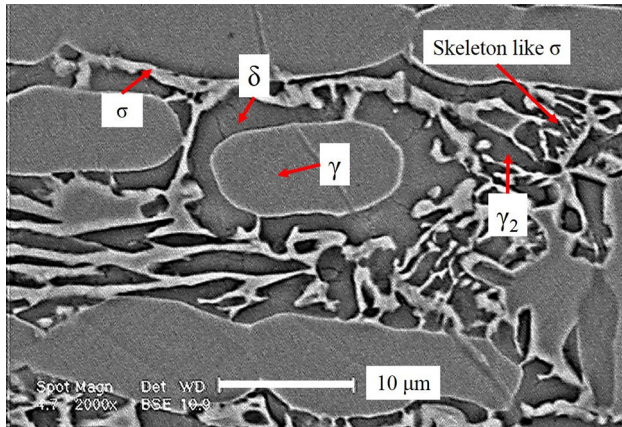


Figure 9 SEM image of the furnace-cooled UNS S32750 super duplex stainless steel of the T-45-F joint. The γ , δ , σ , and γ_2 symbols denote austenite, ferrite, sigma, and secondary austenite phases, respectively.

Table 5 Chemical composition of the phases marked in Fig. 9

Element	Fe	Cr	Mo	Ni	Si
δ	Bal	24.025	6.64	4.86	1.55
γ	Bal	18.97	3.37	10.61	1.34
σ	Bal	26.2	8.41	3.86	1.52
γ_2	Bal	20.42	5.64	9.89	1.29

microstructure of both furnace-cooled and water-cooled AISI 304 SSs.

Mechanical evaluation

Figure 11 presents the microhardness profiles of the samples. The maximum hardness value is approximately 525 Hv and was measured in the centers (NSZs) of T-10-W and T-10-F joints, although the

former's hardness was slightly higher. The high hardness of the NSZs is attributed to the presence of eutectic compounds, which tend to be hard and brittle, in these zones. However, a rise in the holding time caused the hardness figures of these regions to plunge. This phenomenon is linked to the total disappearance of the NSZ from these areas — i.e., the completion of the isothermal solidification. The figures for the samples containing complete ISZs (T-45-W and T-45-F) are similar, approximately 300 Hv.

A noticeable reduction in hardness occurs by moving away from the base metals/interlayer interface toward the base materials. This is because the boron diffusion, i.e., the formation of boride compounds, will dwindle from the base metals/interlayer interface to the inner regions within the base metals. The second highest hardness figure is around 450 Hv, roughly 1.5 as high as the hardness of the DAZ on the AISI 304 SS side (approximately 315 Hv), and was recorded in the DAZs of UNS S32750 SDSSs of all TLP joints. The precipitation of the hard and brittle borides in DAZs is responsible for the high hardness values of these regions. It is worth noting that despite the changes made in the cooling rate, the hardness of ISZ and DAZ remained somewhat unchanged primarily because these regions formed at a constant temperature and thus were not affected by a different cooling process.

According to Fig. 11, the SDSSs in the water-cooled samples have a hardness of 320 ± 4 Hv, which is significantly lower than the hardness of their furnace-cooled counterparts (415 ± 5 Hv). This marked difference between the hardness of the furnace-cooled and water-cooled SDSSs reinforces the formation and presence of the hard secondary phases, particularly the σ phase, in the furnace-cooled SDSSs. The water-

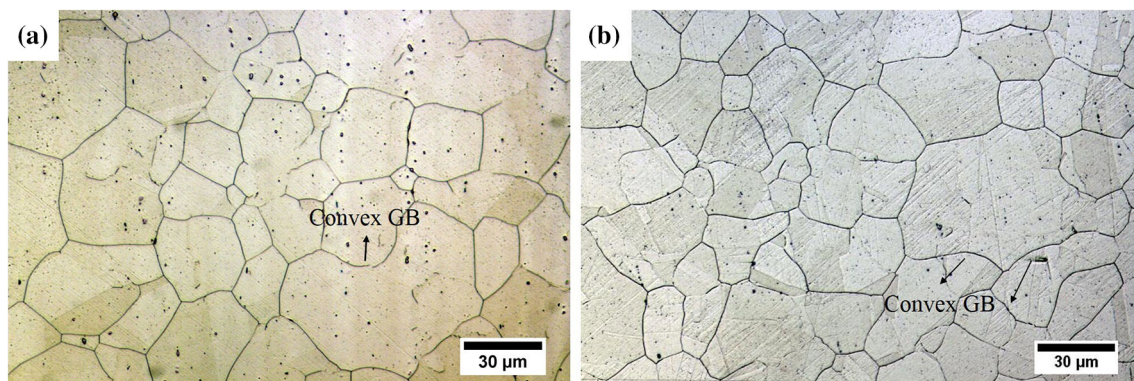
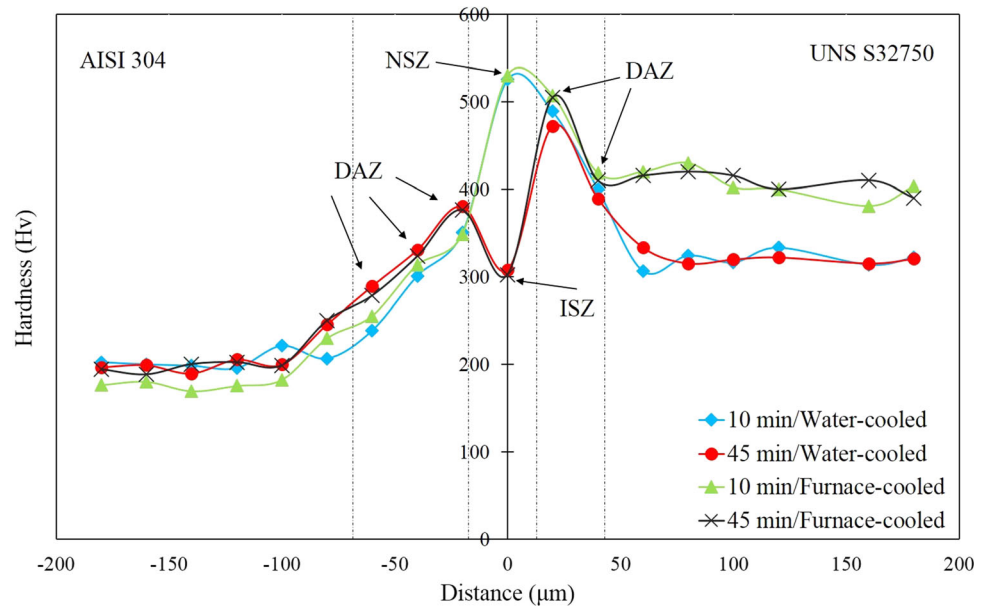


Figure 10 Optical microstructures of **a** the furnace-cooled and **b** the water-cooled AISI 304 stainless steels.

Figure 11 Hardness profiles of the TLP bonds fabricated at 1050 °C.



cooled sample bonded at 1050 °C for 45 min (T-45-W) exhibited the most uniform hardness profile among all TLP joints; however, it did show some inconsistency in its hardness profile caused by the high hardness values of DAZs.

The impacts of the cooling regimes on the mechanical properties of the bonds were studied using shear testing. Figure 12 illustrates the results of the shear tests for joints and base metals. As seen, the shear strength of the TLP bonds notably varies according to the holding time. The joint held at 1050 °C for 10 min with a furnace-cooling (T-10-F) shows the lowest shear strength figure (301 MPa), whereas the joint produced in the similar bonding conditions but with a subsequent water cooling (T-10-W) exhibits slightly better performance and a strength of 332 MPa.

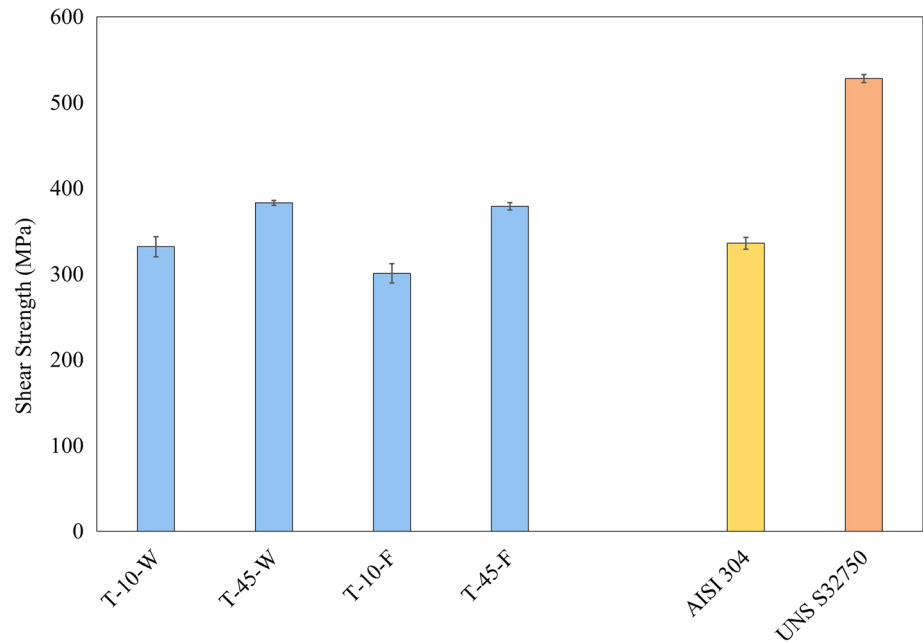
The formation of the brittle intermetallic compounds in the NSZs of both T-10-W and T-10-F samples accounts for their poor mechanical properties. These compounds are proven to act as potential places for crack initiation and can significantly reduce the strength of the TLP bonds [40]. Moreover, a notable improvement in the strength of TLP joints was achieved once the holding time increased to 45 min. Both T-45-W and T-45-F joints possess a shear strength of approximately 380 MPa, which represents around eight-tenth of the strength of the SDSS base metal. The increased shear strength of these two is primarily due to the complete removal of NSZ and the isothermal solidification completion.

Conclusion

Dissimilar transient liquid phase (TLP) bonding of UNS S32750 super duplex stainless steel/BNi-2/AISI 304 stainless steel was conducted at 1050 °C for 10 and 45 min. Once bonding was finished, the joints underwent either furnace-cooling or water-cooling treatments to study how different cooling rates affect the joints' microstructure and mechanical properties. The followings are several conclusions drawn from the present study:

1. In both furnace-cooled and water-cooled TLP joints, a holding time of 45 min was sufficient for the isothermal solidification to complete.
2. The joints held for 10 min consisted of three regions: isothermal solidification zone (ISZ), non-isothermal solidification zone (NSZ), and diffusion-affected zone (DAZ).
3. Regardless of their holding times and cooling conditions, all joints contained ISZ, whose only phase was the γ -Ni solid solution, and DAZs, which mainly consisted of Fe-Cr-Ni-Mo-rich borides.
4. Large Ni-rich and Cr-rich eutectic phases and Ni_3Si solid participates were detected in the NSZ of the furnace-cooled joint, whereas the NSZ of the water-cooled sample contained only minute Ni-rich boride compounds and a γ -Ni solid solution phase.

Figure 12 Shear strength of the TLP bonds, as well as the base metals. W and F denote water-cooling and furnace-cooling regimes, respectively.



- Super duplex stainless steel of the furnace-cooled samples was comprised of γ -austenite, δ -ferrite, and σ -sigma phases. On the other hand, γ -austenite and δ -ferrite phases with an approximately 1:1 ratio existed in the water-cooled ones.
- The average hardness of NSZ was approximately 525 Hv, whereas the hardness of ISZ was 300 Hv. In all bonds, the DAZs of super duplex stainless steel showed a greater hardness (450 Hv) than those of austenitic stainless steel (315 Hv). In the furnace-cooled samples, the hardness of super duplex stainless steel was considerably high, nearly 415 Hv, due to the σ -sigma phase being present in the microstructure. The hardness of the super duplex stainless steels of the water-cooled samples was equal and as high as that of the ISZs. The joint bonded for 45 min with a subsequent water-cooling regime showed the most homogeneous hardness profile.
- With increasing time, the shear strength figures of the TLP bonds improved, irrespective of their cooling conditions. The samples bonded for 45 min possessed the highest shear strength (approximately 380 MPa), having had complete isothermal solidification zones.
- To attain a sound joint between these alloys using a BNi-2 interlayer and to minimize the possible deterioration of the properties of alloys, it is proposed that TLP bonding be performed at

1050 °C, for 45 min, and with subsequent water-cooling treatment.

Acknowledgements

We thank the faculty, employees, and colleagues in the Department of Materials Engineering (Isfahan University of Technology) for their help and support.

References

- Kaladhar M, Subbaiah K, Rao C (2012) Parametric optimization during machining of AISI 304 Austenitic Stainless Steel using CVD coated DURATOMIC cutting insert. *Int J Ind Eng Comput* 3:577–586
- Rodríguez-Martínez JA, Rusinek A, Pesci R, Zaera R (2013) Experimental and numerical analysis of the martensitic transformation in AISI 304 steel sheets subjected to perforation by conical and hemispherical projectiles. *Int J Solids Struct* 50:339–351
- Nilsson J-O, Chai G (1997) The physical metallurgy of duplex stainless steels. *Proc Duplex Stainless Steel* 97:73–82
- Schulz Z, Whitcraft P, Wachowiak D (2014) Availability and economics of using duplex stainless steels. *NACE Corrosion*
- Olsson J, Snis M (2007) Duplex—a new generation of stainless steels for desalination plants. *Desalination* 205:104–113

- [6] Snis M, Olsson J (2008) Reduce costs for storage and distribution of desalted water—use duplex stainless steel. *Desalination* 223:476–486
- [7] Elmer JW, Palmer TA, Specht ED (2007) Direct observations of sigma phase formation in duplex stainless steels using in-situ synchrotron X-ray diffraction. *Metall Mater Trans A* 38:464–475
- [8] Sato YS, Nelson TW, Sterling CJ et al (2005) Microstructure and mechanical properties of friction stir welded SAF 2507 super duplex stainless steel. *Mater Sci Eng A* 397:376–384
- [9] Saidov R, Mourton H, Le Gall R, Saindrenan G (2000) A-TIG welding of UR 52N+ superduplex stainless steel. *Weld Int* 14:633–639
- [10] Hosseini VA, Karlsson L, Engelberg D, Wessman S (2018) Time-temperature-precipitation and property diagrams for super duplex stainless steel weld metals. *Weld World* 62:517–533
- [11] Chiu LH, Hsieh WC, Wu CH (2003) Cooling rate effect on vacuum brazed joint properties for 2205 duplex stainless steels. *Mater Sci Eng A* 354:82–91
- [12] Centeno DMA, Carvalho C Jr, Brandi SD (2015) Brazing of UNS S32101 and UNS S32304 lean duplex stainless steels and UNS S32750 super duplex with AWS A5. 3 BNi-7 (Ni–Cr–P) filler metal. *Weld Int* 29:937–945
- [13] Nilsson J-O (1992) Super duplex stainless steels. *Mater Sci Technol* 8:685–700
- [14] Lu BT, Chen ZK, Luo JL et al (2005) Pitting and stress corrosion cracking behavior in welded austenitic stainless steel. *Electrochim Acta* 50:1391–1403
- [15] Esmaeili H, Mirsalehi SE, Farzadi A (2018) Vacuum TLP bonding of Inconel 617 superalloy using Ni–Cr–Si–Fe–B filler metal: metallurgical structure and mechanical properties. *Vacuum* 152:305–311
- [16] Norouzi E, Atapour M, Shamanian M, Allafchian A (2016) Effect of bonding temperature on the microstructure and mechanical properties of Ti–6Al–4V to AISI 304 transient liquid phase bonded joint. *Mater Des* 99:543–551
- [17] Jalali A, Atapour M, Shamanian M, Vahman M (2018) Transient liquid phase (TLP) bonding of Ti–6Al–4V/UNS 32750 super duplex stainless steel. *J Manuf Process* 33:194–202
- [18] Cook GO, Sorensen CD (2011) Overview of transient liquid phase and partial transient liquid phase bonding. *J Mater Sci* 46:5305–5323. <https://doi.org/10.1007/s10853-011-5561-1>
- [19] MacDonald WD, Eagar TW (1992) Transient liquid phase bonding. *Annu Rev Mater Sci* 22:23–46
- [20] Ghaderi S, Karimzadeh F, Ashrafi A (2020) Evaluation of microstructure and mechanical properties of transient liquid phase bonding of Inconel 718 and nano/ultrafine-grained 304L stainless steel. *J Manuf Process* 49:162–174
- [21] Jafari M, Rafiei M, Mostaan H (2019) Effect of solidification mode on microstructure and mechanical properties of AISI420 steel to SAF2507 steel dissimilar joint produced by transient liquid phase. *Met Mater Int* 1–12
- [22] Abdolvand R, Atapour M, Shamanian M, Allafchian A (2017) The effect of bonding time on the microstructure and mechanical properties of transient liquid phase bonding between SAF 2507 and AISI 304. *J Manuf Process* 25:172–180
- [23] Pohl M, Storz O, Glogowski T (2005) Effect of sigma-phase morphology on the properties of duplex stainless steels. *Microsc Microanal* 11:230–231
- [24] Shirdel M, Mirzadeh H, Parsa MH (2014) Abnormal grain growth in AISI 304L stainless steel. *Mater Charact* 97:11–17
- [25] Mosallae M, Babanejhad A (2020) Correlation between microstructure and pitting corrosion behavior of TLP bonded DSS-2205/Ni–P/DSS-2205 specimens. *Met Mater Int* 1–11
- [26] Mirzaei S, Binesh B (2020) Microstructure evolution mechanism and corrosion behavior of transient liquid phase bonded 304L stainless steel. *Met Mater Int* 1–15
- [27] Arafin MA, Medraj M, Turner DP, Bocher P (2007) Effect of alloying elements on the isothermal solidification during TLP bonding of SS 410 and SS 321 using a BNi-2 interlayer. *Mater Chem Phys* 106:109–119
- [28] Rhee B, Roh S, Kim D (2003) Transient liquid phase bonding of nitrogen containing duplex stainless steel UNS S31803 using Ni–Cr–Fe–Si–B insert metal. *Mater Trans* 44:1014–1023
- [29] A923-14 A (2014) Standard Test Methods for Detecting Detrimental Intermetallic Phase in Duplex Austenitic/Ferritic Stainless Steels
- [30] Jamaloei AD, Khorram A, Jafari A (2017) Characterization of microstructure and mechanical properties of dissimilar TLP bonding between IN718/IN600 with BNi-2 interlayer. *J Manuf Process* 29:447–457
- [31] Gale WF, Butts DA (2004) Transient liquid phase bonding. *Sci Technol Weld Join* 9:283–300
- [32] Baker H, Okamoto H (1992) ASM handbook. Vol. 3. Alloy Phase Diagrams. ASM International, Materials Park, Ohio 44073-0002, USA, 1992 501
- [33] Xu C-H, Gao W, Yang Y-L (2001) Superplastic boronizing of a low alloy steel—microstructural aspects. *J Mater Process Technol* 108:349–355
- [34] He Q, Zhu D, Dong D et al (2019) Effect of bonding temperature on microstructure and mechanical properties during TLP bonding of GH4169 superalloy. *Appl Sci* 9:1112–1121
- [35] Dezfooli MS, Shamanian M, Golzar MA (2021) The effect of bonding time on the microstructure and mechanical properties of dissimilar transient liquid phase bonding between UNS N08825 alloy and UNS S32750 super duplex

- stainless steel using the BNi-2 interlayer. *J Manuf Process* 64:464–472
- [36] Idowu OA, Ojo OA, Chaturvedi MC (2006) Microstructural study of transient liquid phase bonded cast Inconel 738LC superalloy. *Metall Mater Trans A* 37:2787–2796
- [37] Sathirachinda N, Pettersson R, Wessman S, Pan J (2010) Study of nobility of chromium nitrides in isothermally aged duplex stainless steels by using SKPFM and SEM/EDS. *Corros Sci* 52:179–186
- [38] Jiang ZL, Chen XY, Huang H, Liu XY (2003) Grain refinement of Cr25Ni5Mo1.5 duplex stainless steel by heat treatment. *Mater Sci Eng A* 363:263–267
- [39] Hsieh C-C, Wu W (2012) Overview of intermetallic sigma (?) phase precipitation in stainless steels. *ISRN Metall* 2012
- [40] Pouranvari M, Ekrami A, Kokabi AH (2014) Diffusion brazing metallurgy of IN718/Ni–Cr–Si–B–Fe/IN718. *Weld J* 93:60–68

Publisher's Note Springer Nature remains neutral with regard to jurisdictional claims in published maps and institutional affiliations.